ELSEVIER

Contents lists available at ScienceDirect

# **Materials Letters**

journal homepage: www.elsevier.com/locate/matlet



# Ballistic impact testing of acrylic and alumina thin-films

Vignesh Mahalingam 👨 \*, Raghavan Ranganathan 👨

IIT Gandhinagar, Department of Materials engineering, IIT Gandhinagar, Gandhinagar, 382355, Gujarat, India

# ARTICLE INFO

Keywords: Molecular dynamics simulation Ballistic impact PMMA  $\alpha\text{-Al}_2O_3$ 

#### ABSTRACT

High velocity projectiles cause damage to critical structures in space. Many of them travel at speeds of a few km/s to several hundred km/s. Such projectiles can punch through aircraft. In addition, bullets from modern weapons might reach 2.5 km/s. Spherical diamond projectiles are tested against Poly-Methyl-Metha-Acrylate (PMMA) and single-crystal corundum alumina ( $\alpha$ -Al<sub>2</sub>O<sub>3</sub>) thin films. PMMA is created from two configurations: random and oriented along impact direction. The penetration velocity (V<sub>50</sub>) of PMMA and  $\alpha$ -alumina are found to be near 400 m/s and 4.5 km/s, respectively. This study indicates that PMMA sandwiched between two layers of alumina can be produced, with a thickness that can be calculated using specific penetration energies ( $E_p^*$ ) from the projectile radius, to stop most projectiles effectively.

#### 1. Introduction

Molecular dynamics (MD) simulations have been effective studying impact at mesoscale using nanoscale projectiles and thin films [1,2]. Bioinspired PMMA- $\alpha$ -Al<sub>2</sub>O<sub>3</sub> composites are considered to have superior mechanical properties than their individual components and their nacre counterparts [3,4]. When a spherical projectile of radius R and density  $\rho_{\rm p}$  hits a film of height h and density  $\rho_{\rm f}$ , an impact zone (IPZ) larger than the size of the projectile is created [1]. This is given as

$$r_{IPZ} \approx R + 0.8R \sqrt{\frac{\rho_p}{\rho_f} \cdot \frac{R}{h}}$$
 (1)

As one can see from Eq. (1) that the ratio of projectile and film density and that of R and h can control IPZ size.  $\frac{R}{h} < 1$  can have nonpenetrating scenarios [5]. It is sufficient to have  $\frac{R}{h} = 1$  for an efficient simulation. A spherical projectile having diamond lattice with lattice constant 3.567 Å, density  $\rho_p = 3527~kg/m^3$ . The densities of PMMA and alumina thin films were  $\rho_{PMMA} = 1130~kg/m^3$  and  $\rho_\alpha - Al_2O_3 = 3860~kg/m^3$ , respectively. For PMMA, using Eq. (1) the impact zone radius is calculated as  $r_{PMMA-IPZ} = 2.4R$ . PMMA thin film has h=10 nm were created with side length 60 nm, greater than that of calculated IPZ diameter. For alumina, using Eq. (1), the impact zone radius is calculated as  $r_{alumina-IPZ} = 1.76R$ . Alumina thin films have thickness h=1.3 nm and a square side of 15 nm, greater than that of calculated IPZ radius.

#### 2. Computational methodology

All MD simulations in this work were run using Large-scale Atomic/Molecular Massively Parallel Simulator (LAMMPS) [6]. Corundum α-Al<sub>2</sub>O<sub>3</sub> is the most stable form of alumina and has a trigonal structure belonging to R3c space group (167). It has a lattice constant of a=b=4.761 Å in two directions and c=12.995 Å. For  $\alpha$ -alumina, a third-generation Charge-Optimized Many-Body (COMB3) is used [7]. The timestep in all simulations is 1 fs. A recently developed Coarse-Grained (CG) forcefield is used [8] for MD simulation of PMMA. Initially, a 100-monomer polymer chain was created. 80 such chains were randomly aligned like spherocylinders in non-overlapping fashion using a large cutoff of 30 Å [9]. The CG PMMA films are subjected to energy minimization and were equilibrated at 750 K, 100 atm pressure Nosé-Hoover (NPT) dynamics for 5 ns and brought down to room temperature and pressure as mentioned in the original work [8]. This creates a 10 nm cubic box with the converged PMMA density, referred to as PMMA bulk in Fig. 1. PMMA films of dimensions  $60 \times 60 \times 10$  nm (length x width x height) are obtained by replicating this box in x and y directions. Edge effects were taken care during thin film preparation. For studying impact dynamics, the top and bottom surfaces of PMMA is smoothed using a fix wall technique like previous works [10,11]. The residual velocity, V<sub>r</sub> is the steady-state velocity reached either after penetration of the target, or after rebounding from the target in a nonpenetrating scenario. If the projectile penetrates the target, it exists with a positive velocity V<sub>r</sub> less than impact velocity V<sub>i</sub>. This is like  $V_{50}$  velocity at which 50% of projectiles penetrate. The difference in

E-mail addresses: vignesh.mahalingam@iitgn.ac.in (V. Mahalingam), rraghav@iitgn.ac.in (R. Ranganathan).

<sup>\*</sup> Corresponding author.

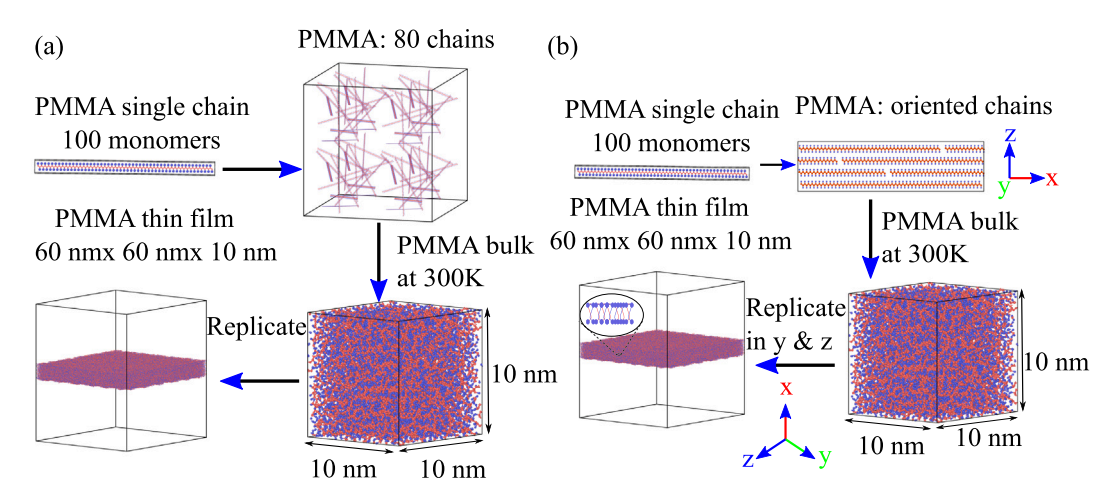


Fig. 1. PMMA thin film generation and equilibration from (a) random and (b) oriented configuration.

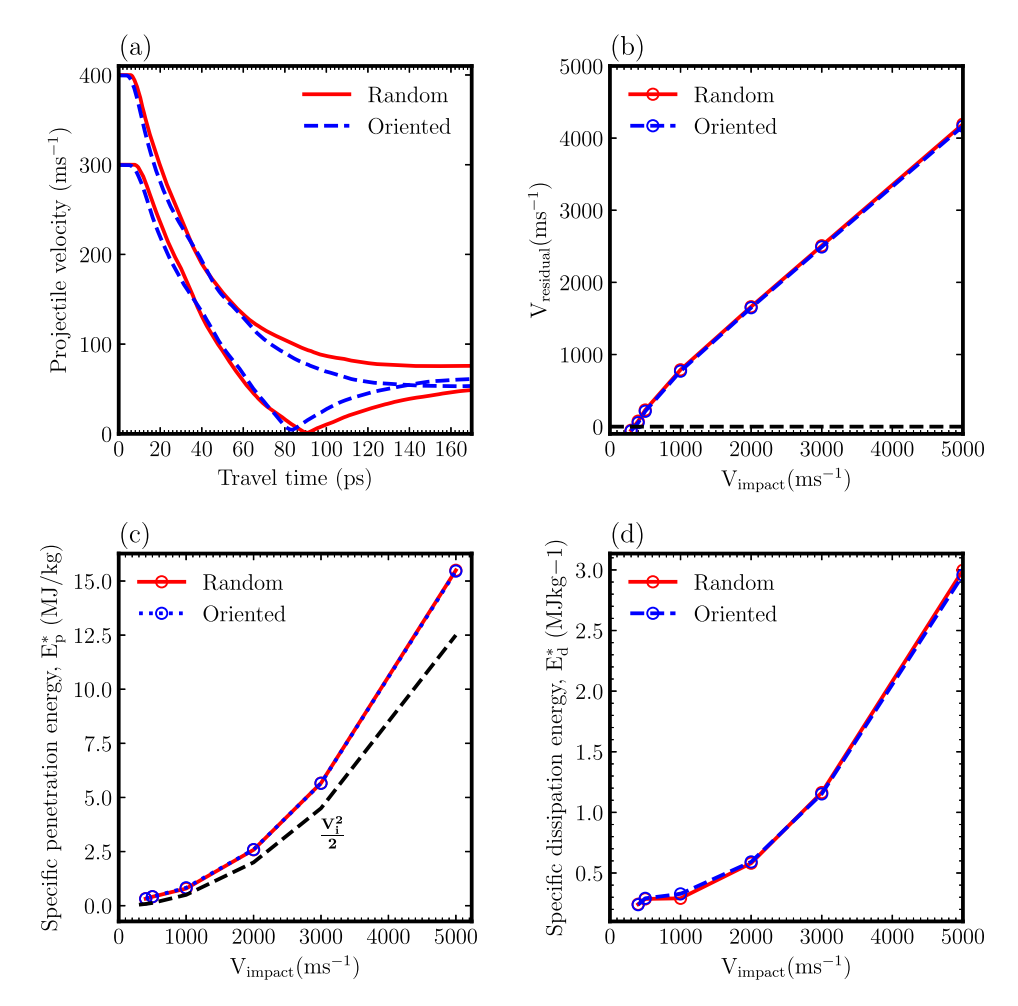


Fig. 2. Residual velocity of projectile as a function of impact velocity (a) before (300 m/s) and after  $V_{50}$  velocity (400 m/s), (b) residual velocities of projectile as a function of impact velocities, (c) Specific penetration energy ( $E_p^*$  (MJ/kg)) as a function of impact velocity and (d) Specific dissipation energy ( $E_d^*$  (MJ/kg)) as a function of impact velocity.

kinetic energy  $E_k$  of the projectile is referred to as penetration energy  $(E_p)$  and is given as

$$E_p = \Delta E_k = \frac{1}{2} \cdot m_{proj} \cdot (V_i^2 - V_r^2)$$
 (2)

If  $E_p$  in Eq. (2) is scaled by the mass of the thin film directly under projectile, then it is referred to as specific penetration energy  $E_p^*$ . The mass of the thin film under projectile impact is given as  $m_{film} = 1$ 

 $ho_{film}\cdot V_{film}$ . In all previous works, the volume  $V_{film}$  is considered as a cylinder with a radius of projectile (R) and height h. If R=h, then  $m_{film}=\rho_{film}\cdot\pi\cdot R^2\cdot h=\rho_{film}\cdot\pi\cdot R^3$ . The specific penetration energy is given as

$$E_p^* = \frac{\Delta E_k}{m_{film}} \approx \frac{v_i^2}{2} + E_d^* \tag{3}$$

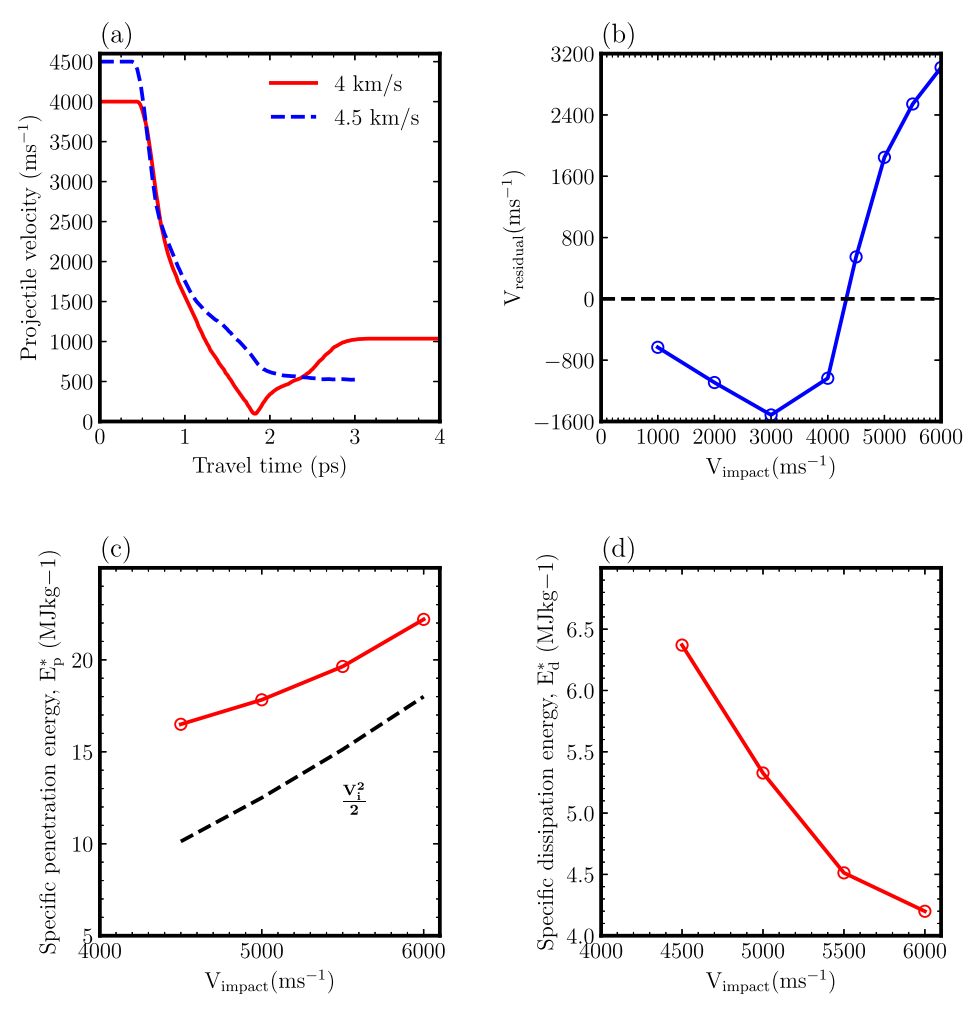


**Fig. 3.** Residual velocity of projectile as a function of impact velocity (a) before (4 km/s) and after  $V_{50}$  velocity (4.5 km/s) for α-Al<sub>2</sub>O<sub>3</sub>, (b) residual velocities of projectile as a function of impact velocities and (c) Specific penetration energy ( $E_p^*$  (MJ/kg)) as a function of impact velocity and (d) Specific dissipation energy ( $E_d^*$  (MJ/kg)) of α-Al<sub>2</sub>O<sub>3</sub> as a function of impact velocity.

, where  $E_d^*$  is specific dissipation energy due to the absorption/ dissipation response of the target thin film to the incoming projectile.  $E_d^*$  can be obtained by subtracting from  $E_p^*$ , the first term in Eq. (3).

### 3. Results and discussion

# 3.1. Impact of projectile on PMMA

The residual velocities V<sub>r</sub> of the diamond projectile after impact coming with different initial impact velocities V<sub>i</sub> were obtained by tracking projectile velocity with time as shown in Fig. 2(a). The  $V_{50}$ velocity for PMMA is between 300 and 400 m/s (Fig. 2(b)). In addition, PMMA chains oriented along impact direction were analyzed (Fig. 1(b)). The residual velocities, for different impact velocities, of the oriented films were lower than random films. Nevertheless, the differences were negligible (Fig. 2(b)). The  $V_{50}$  velocity also remained the same (Fig. 2(b)). The specific penetration energy  $E_n^*(MJ/kg)$  increases non-linearly as impact velocity  $V_{impact}$  (Fig. 2(c)). For oriented PMMA thin-films, the specific penetration energy  $E_n^*(MJ/kg)$  (Fig. 2(c) and the specific dissipation energy  $E_d^*(MJ/kg)$  are close to their random counterparts (Fig. 2(d)). The temperature of the film target is tracked by defining a circular region of diameter 60 nm (side of square film). Evolution of the temperatures is plotted in Figs. 4(a)-(b) for random PMMA thin-films and in Figs. 4(c)-(d) for oriented ones. The peak temperatures of oriented films (2628 K), were significantly lower than 5450 K, for random films (Fig. 4(g)) at 5 km/s. This is due to anisotropic heat transfer as bond alignment is along the projectile direction.

### 3.2. Impact of projectile on alumina

The  $V_{50}$  velocity for  $\alpha$ -Al<sub>2</sub>O<sub>3</sub> is found to be between 4 and 4.5 km/s (Fig. 3(a)). Monolayer graphene has a  $V_{50}$  velocity of 2.2 km/s [1,10].  $E_p^*(MJ/kg)$  of graphene layers is below 15 MJ/kg at 4.5 km/s [1].  $\alpha$ -alumina has  $E_p^*(MJ/kg)$  of 16.5 MJ/kg at 4.5 km/s (Fig. 3(c)).  $\alpha$ -alumina outperforms graphene. Fig. 3(b) shows the residual velocities  $V_r$  of diamond projectile after impact with  $\alpha$ -Al<sub>2</sub>O<sub>3</sub> initially traveling with different initial velocities  $V_i$ . The specific dissipation energy  $E_d^*(MJ/kg)$  decreases after the  $V_{50}$  velocity of 4.5 km/s to 6 km/s (Fig. 3(d)). The temperature of  $\alpha$ -alumina film target is tracked by defining a circular region of diameter 15 nm (side of square film) (Fig. 4(e),(f)). The peak temperatures are less than that of PMMA, even at higher velocities (Fig. 4(g)).

#### 4. Outlook and conclusion

The ballistic impact studies of diamond projectiles on PMMA and alumina thin films were done using all atom MD simulations. The specific penetration energy  $(E_p^*)$  of the PMMA and  $\alpha$ -Al<sub>2</sub>O<sub>3</sub> thin films at V<sub>50</sub> velocity of were 0.323 MJ/kg and 16.495 MJ/kg, respectively. The decrease of projectile velocity from 4.5 km/s to a residual velocity  $(V_r)$  of 576 m/s shows  $\alpha$ -alumina's potential in ballistic-resistant applications. PMMA has a low density of 1130 kg/m³,  $\alpha$ -alumina has a high density of 3860 kg/m³. Whilst, random and oriented PMMA thin films heats up to 5450 K and 2628 K under impact at 5 km/s,  $\alpha$ -Al<sub>2</sub>O<sub>3</sub> heats

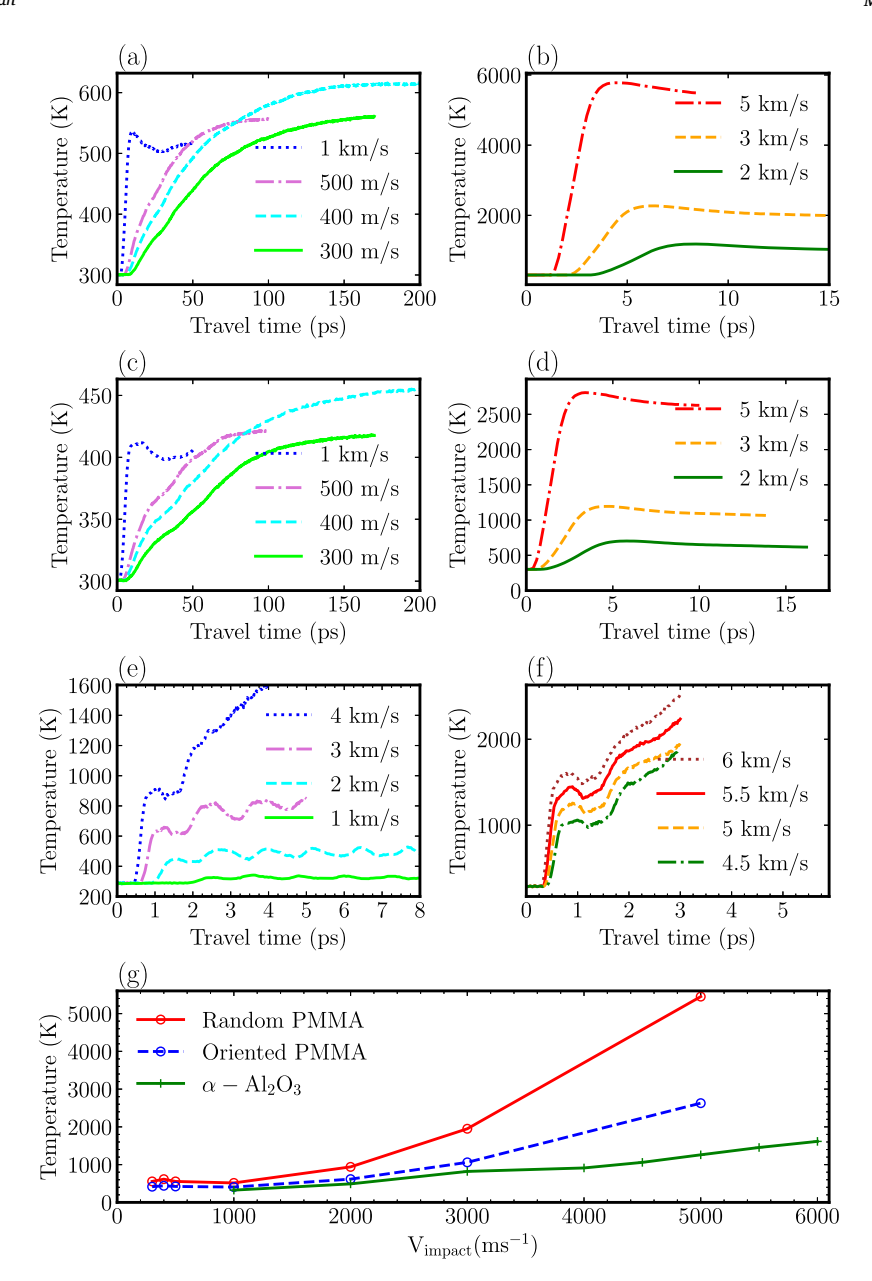


Fig. 4. Temperature as a function of simulation time for impact velocities (a) before and (b) after 1 km/s for random PMMA films, (c) before and (d) after 1 km/s for oriented PMMA thin films, (e)  $\alpha$ -Al<sub>2</sub>O<sub>3</sub> temperature as a function of simulation time for impact velocities before and (f) after 4 km/s, (g) peak temperature of PMMA and  $\alpha$ -Al<sub>2</sub>O<sub>3</sub> as a function of impact velocity.

up to  $1615~\rm K$ . The prospect of a composite with PMMA sandwiched between alumina thin films for a better and lightweight ballistic-resistant material at larger length scales entails further investigation.

## CRediT authorship contribution statement

**Vignesh Mahalingam:** Writing – original draft, Validation, Methodology, Investigation, Formal analysis, Data curation, Conceptualization. **Raghavan Ranganathan:** Resources, Project administration, Funding acquisition.

### Declaration of competing interest

The authors declare that they have no known competing financial interests or personal relationships that could have appeared to influence the work reported in this paper.

### Acknowledgments

The authors thank the Department of Science and Technology (DST), Ministry of Science, India, for funding the project through the grant CRG/2023/005333. The authors acknowledge the PARAM Ananta supercomputing facility for all the simulations reported in this work.

### Appendix. Supporting information

Supporting information associated with this article can be found online at:

- · Videos of ballistic impact of diamond projectile on PMMA
- Videos of ballistic impact of diamond projectile on α-Al<sub>2</sub>O<sub>3</sub>

#### Data availability

Data will be made available on request.

#### References

- Z. Meng, S. Keten, Unraveling the effect of material properties and geometrical factors on ballistic penetration energy of nanoscale thin films, J. Appl. Mech. 85 (12) (2018) 121004, http://dx.doi.org/10.1115/1.4041041.
- [2] A. Giuntoli, N.K. Hansoge, S. Keten, Star topology increases ballistic resistance in thin polymer films, Extrem. Mech. Lett. 41 (2020) 101038, http://dx.doi.org/10.1016/j.eml.2020.101038, URL https://www.sciencedirect.com/science/article/pii/S2352431620302467.
- [3] R.P. Behera, H. Le Ferrand, Impact-resistant materials inspired by the mantis shrimp's dactyl club, Matter 4 (9) (2021) 2831–2849, http://dx.doi.org/10. 1016/j.matt.2021.07.012, URL https://www.sciencedirect.com/science/article/ pii/\$2590238521003593.
- [4] E. Munch, M.E. Launey, D.H. Alsem, E. Saiz, A.P. Tomsia, R.O. Ritchie, Tough, bio-inspired hybrid materials, Science 322 (5907) (2008) 1516–1520, http://dx.doi.org/10.1126/science.1164865, arXiv:https://www.science.org/doi/ pdf/10.1126/science.1164865. URL https://www.science.org/doi/abs/10.1126/ science.1164865.

- [5] P.P. Singh, R. Ranganathan, Superior impact resistance conferred by hierarchical nacre-inspired nanocomposites: A molecular dynamics study, Carbon 233 (2025) 119885, http://dx.doi.org/10.1016/j.carbon.2024.119885, URL https:// www.sciencedirect.com/science/article/pii/S0008622324011047.
- [6] S. Plimpton, Fast parallel algorithms for short-range molecular dynamics, J. Comput. Phys. 117 (1) (1995) 1–19, http://dx.doi.org/10.1006/jcph.1995.1039, URL https://www.sciencedirect.com/science/article/pii/S002199918571039X.
- [7] K. Choudhary, T. Liang, A. Chernatynskiy, S.R. Phillpot, S.B. Sinnott, Charge optimized many-body (COMB) potential for Al2o3 materials, interfaces, and nanostructures, J. Phys.: Condens. Matter. 27 (30) (2015) 305004, http://dx. doi.org/10.1088/0953-8984/27/30/305004.
- [8] D.D. Hsu, W. Xia, S.G. Arturo, S. Keten, Systematic method for thermomechanically consistent coarse-graining: a universal model for methacrylate-based polymers, J. Chem. Theory Comput. 10 (6) (2014) 2514–2527, http://dx.doi. org/10.1021/ct500080h.
- [9] C. Ferreiro-Córdova, J.S. Van Duijneveldt, Random packing of hard spherocylinders, J. Chem. Eng. Data 59 (10) (2014) 3055–3060, http://dx.doi.org/10.1021/ie500119r.
- [10] A.L. Bowman, E.P. Chan, W.B. Lawrimore, J.K. Newman, Supersonic impact response of polymer thin films via large-scale atomistic simulations, Nano Lett. 21 (14) (2021) 5991–5997, http://dx.doi.org/10.1021/acs.nanolett.1c00961.
- [11] A.L. Bowman, W.A. Pisani, M. Shukla, Enhanced impact resistance in multilayered polymer–graphene nanocomposites via confinement, ACS Appl. Eng. Mater. (2025) http://dx.doi.org/10.1021/acsaenm.4c00808.